35th Symposium on Naval Hydrodynamics
Nantes, France, 7 July - 12 July 2024

Ship wake scaling: comparison between RANS CFD predictions and more traditional empirical methods

A.R. Starke[1], S. Shingo[2], D. Villa[3], H. Yoon[4], R. Broglia[5], K.J. Maki[6], K. E. Marlantes[6], P. Horn[7], Y. Jiang[8], F. Zhao[9], J. Banks[10] and B. Winden[11]

([1]Maritime Research Institute Netherlands (MARIN), The Netherlands, [2]Shipbuilding Research Centre of Japan (SRCJ), Japan, [3]University of Genova (UniGe), Italy, [4]IIHR – Hydroscience & Engineering, Iowa, USA, [5]Consiglio Nazionale delle Ricerche (CNR), Italy, [6]University of Michigan (UM), Michigan, USA, [7]Hamburgische Schiffbau-Versuchsanstalt GmbH (HSVA), Germany, [8]Dalian University of Technology (DUT), China, [9]China Ship Scientific Research Centre (CSSRC), China, [10]University of Southampton (UoS), UK, [11]SHORTCUT CFD LLC, Bryan, Texas, USA; Texas A&M University, Department of Ocean Engineering, College Station Texas, USA)

ABSTRACT

RANS CFD predictions of the full-scale and model-scale wake fraction of 14 different ships, analyzed by 9 different institutes and 7 different CFD codes, are compared to more traditional empirical wake-scaling methods such as the ITTC78 formula and the Yazaki method. Since most empirical methods are based on potential flow considerations, CFD is also used to compute the potential wake of each ship. For the ITTC method, and the Sasajima-Tanaka method on which it is based, the validity of the assumptions underlying these empirical methods are investigated and it was found that not all underlying assumptions were supported by the CFD. This holds especially for the assumed proportionality between the scale effect on the friction coefficient and the scale effect on the wake fraction. As a consequence, the present CFD results consistently predict lower full-scale wake fractions than the empirical methods for all ships considered.

INTRODUCTION

Understanding of the ship wake is critical to design an efficient and quiet propeller. The ship wake is characterized by the viscous flow at high Reynolds number over somewhat smooth hulls that have a wide range of turbulence scales that range from the Kolmogorov scale up to those of the vortices that are shed from the bow and upstream appendages such as shafts, struts, skegs and bilge keels. With few exceptions our understanding of full-scale wakes is based off computation or experiment of model wakes, and the extrapolation over several decades of Reynolds number introduces significant uncertainty in the prediction of full-scale performance.

Nowadays, several wake scaling methods are in use to extrapolate wake fractions and wake fields that have been obtained from model testing to ship scale. These extrapolation methods are typically based on assumed general relations between scale effects on wake fractions and friction coefficients, such as in the ITTC78 procedure (ITTC, 1978), or on regression analysis of historical full scale data, such as in the Yazaki method (Yazaki, 1969).

Various campaigns have been reported in the literature to collect full-scale wake (beyond those used by Yazaki), but given the effort and expenses required to collect wake field data at full scale, the number of ships and ship types for which full-scale detail will become available is extremely limited. Furthermore, for new ships and propellers, it is rarely feasible to build prototypes for measurement purposes. Thus the extrapolation to full-scale of model-scale experimental measurement is the standard practice.

CFD of course offers the possibility to compute wakes at either model or full scale Reynolds number. Direct computation at full scale is attractive because it avoids extrapolation, but the primary drawback is the difficulty to estimate the quality of the solution since validation data is so sparse. CFD computation at model scale is more easily validated, and has been the subject of many international CFD workshops. If CFD is done at model scale, it must still be extrapolated with some suitable method. The objective of this paper

is to use CFD performed at model and full scale to investigate the extrapolation of ship wakes from model scale information.

The majority of the authors of this paper are members of the Specialist Committee on Combined CFD and EFD Methods of the 30th ITTC, and consequently the ITTC78 wake scaling formula is taken as starting point to guide the analysis, where the three main assumptions underlying this wake scaling method are tested using CFD.

In the ITTC78 method the wake is decomposed in a potential component and a frictional component. Specifically it is assumed that:

- The potential part of the wake fraction is proportional to the potential part of the thrust deduction
- The scale effect on the frictional part of the thrust deduction is small
- The scale effect on the wake fraction is principally determined by a function of the scale effect on the friction coefficient

In order to analyze these assumptions, the authors have used different CFD codes to compute the double-body flow around various ships. All authors have computed the flow at model scale and full scale Reynolds number. The separation into potential and frictional parts is done by also computing the potential wake. To obtain the potential part of the wake and the thrust deduction, the no-slip boundary condition imposed on solid walls in the viscous-flow computations at model and full-scale Reynolds number was replaced by a free-slip boundary condition. Consequently, the turbulence model is not activated and turbulence eddy-viscosity levels and friction resistance are practically zero. The corresponding solution is considered as an approximation of a potential-flow, or an Euler solution. While this is not strictly true since the CFD results have discretization error that behaves in the same manner as viscous diffusion, it is assumed to be a suitable approximation and it is convenient to use the same solver and computational meshes that were employed for the viscous-flow solutions.

Some participants also computed the effective wake and thrust deduction. A secondary important focus of this work is the estimation of numerical uncertainty. The authors computed solutions on multiple grids and employed the Eça and Hoekstra (2014) least-squares method to estimate uncertainties on the wake fraction, friction coefficient. Additionally the uncertainty is propagated through the extrapolation process to quantify uncertainty at full scale.

OVERVIEW OF THE COMPUTATIONS

RANS-based resistance and wake field predictions have been made both for potential flow and for model and full-scale Reynolds number by 9 participants for 14 different ships. These include several container ships, tankers and the ONR Tumblehome. Three well-known cases, namely KCS, KVLCC2 and JBC, have been computed by multiple participants. For four ships different speeds or ballast conditions have been analyzed. DUT/CSSRC have contributed the YUPENG container ship and both MARIN and UniGe have contributed a number of cases that for reasons of confidentiality cannot be further specified. They will simply be referred to as ‘tankers’ and ‘container ships’. Table 1 lists the ships that have been analyzed by multiple participants.
Both UniGe, CNR-INM and MARIN have performed power predictions for both potential flow and model and full-scale Reynolds number to determine thrust deduction fractions. These power predictions have been performed at the ship self-propulsion point and the inviscid flow computations at equal thrust compared to the corresponding model or full-scale viscous-flow computation.

Table 1: Cases analyzed by multiple participants

	KCS	JBC	KVLCC2
MARIN	V	V	V
UniGe	V	V	V
SRCJ	V	V	V
CNR-INM	V	V	-
UoS / SC	-	-	V
UM	-	-	V
HSVA	V	V	V
DUT / CSSRC	V	V	-

To reduce the computational effort computations have been performed ignoring ship wave making (the double-body approach).

COMPUTATIONAL METHODS

The results discussed in the next section have been obtained using various RANS-based CFD codes by a number of institutes.

Institute	Software or code name
CNR-INM	OpenFOAM
CSSRC	NaViiX
DUT	StarCCM+
HSVA	FreSCo+
MARIN	PARNASSOS
SRCJ	NAGISA

UM	HELYX
UniGe	OpenFOAM
UoS	OpenFOAM

MARIN

The RANS solver used is PARNASSOS, a code developed and used by MARIN and IST. It solves the discretised Reynolds-averaged Navier-Stokes equations for a steady, 3D incompressible flow around a ship's hull, using structured HO-type meshes. Various eddy-viscosity turbulence models are available. For all the computations in this paper the one-equation turbulence model of Menter was used. The model was extended with a correction for the longitudinal vorticity. The discretisation is of finite-difference type. The momentum and continuity equations are solved in fully coupled form. Therefore, the continuity equation need not be recast in a pressure correction or pressure Poisson equation, but can simply be solved as it is. After discretisation and linearisation, the three momentum equations and the continuity equation give rise to a matrix equation containing 4*4 blocks, which is solved using preconditioned GMRES. This fully coupled solution has been found to be robust and quite insensitive to the mesh aspect ratio. This allows solving the discretized equations on extremely contracted grids close to the wall. As a result, wall functions are not necessary, not even at full scale.

For the analysis of the flow past the propeller, use is made of a boundary element method (BEM) that solves the incompressible potential flow equations for lifting and non-lifting bodies. The method, designated PROCAL, is being developed within MARIN's Cooperative Research Ships (CRS) for the unsteady analysis of cavitating propellers operating in a prescribed ship wake. It has been validated for open water characteristics, shaft forces, sheet cavitation inception and extent and hull pressure fluctuations. The code is a low order BEM that solves for the velocity disturbance potential.

The steady RANS solver and the unsteady boundary element method are coupled in the following way. First a RANS computation is made for the case without propeller. This provides the resistance and the nominal wake field at the propeller plane. Then, in this wake field a first propeller computation is made using the BEM, iteratively updating the propeller RPM to a prescribed thrust coefficient. This provides a thrust- and loading distribution. This unsteady loading distribution, in a ship-fixed coordinate system, is averaged in time for all blade positions to produce a steady, but axially, circumferentially and radially non-uniform force distribution. This is interpolated to the RANS grid. Finally the viscous-flow computation is restarted from the previous solution, imposing the loading distribution from the BEM as a force field acting on the flow. This yields a new total wake field, from which we then subtract the induced velocities coming from the BEM to obtain a first estimate of the effective wake field. Then an iteration is performed between both methods until changes in the RPM and torque coefficients and the effective inflow to the propeller have become negligibly small.

University of Genova

The RANS solver considered is the open-source OpenFOAM code. It is a general-purpose finite volume-based 3-D viscous code that handles unstructured polyhedral meshes. It includes turbulence effects using various models (such as LES, DES or RANS models), and in the present work, the widely used two-equation Shear-Stress Transport (SST) k-omega model is used. The marine community widely uses this model to handle ship resistances and wake evaluation simulations. Due to the nature of the problem, a steady-state solver has been adopted with bounded second-order accurate schemes for all the equations.

To reduce the computational costs, proper prism-layer mesh has been designed around the solid body able to guarantee a y+ on the wall surfaces useful for the adopted wall-functions. The mesh generator realizes an average y+ close to 100 at the model scale and higher (around 1000) at the full scale. Even if at full scale, this value is quite high, it is still proper due to the highly regular flow around the hull at full scale. However, these values are necessary to reduce the overall computational costs and to guarantee proper code stability also for these computations.

The adopted grid layout is built with an unstructured hex-dominant cartesian mesh generator (Juretić, 2015) on a parallelepiped domain: the inlet boundary condition has been located at a distance of 1.5 times the ship length (Lpp) in front of the ship, the outlet at 2.5Lpp in the streamwise direction and the side boundaries, considered as slip walls (no shear stresses can occur) are located at 1Lpp far from the hull body. These sizes have been selected to reduce as much as possible the boundary interactions on the results, to represent an open water condition better. The adopted mesh size uses far-field cells with a size of 0.1Lpp and four standard box refinements up to the near body region and a further surface refinement on the body itself, generating cells with a size of about 0.003Lpp on the hull. On the stern region, where the propeller

takes place, further refinements have been considered, reducing the cell size up to 0.0008Lpp. This layout generates a mesh of about 2 million cells (the cell count slightly changes based on the considered model).

A body-force approach is used to include the propeller effect in the viscous computation. This approach guarantees the application of the correct thrust (increased due to the interaction factors) in a simple and fast way. On the contrary, even if the equilibrium thrust can be extracted, the propeller revolution rate cannot be directly evaluated. To overcome this issue and, consequently, to evaluate the effective wake fraction, an already successfully adopted procedure is considered (Villa, Gaggero et al. 2019). This procedure extracts the wakefield into the propeller disk when the body forces are active; then, by subtracting the self-induced velocities coming from a separate viscous calculation where only the body forces are included, the effective wake can be straightforwardly obtained.

This procedure can also be adopted by considering different force distributions, like radial or radial and circumferential force distributions, without significantly affecting the self-propulsion results (Villa, Gaggero et al. 2019). The main differences arise only in the shape of the slipstream flow and, consequently, affect only the device located inside it (Bruzzone, et al. 2014). Considering that the correct distribution is known only by knowing the propeller geometry, for the sake of simplicity, in the present analyses, a constant distribution is preferred.

SRCJ

The RANS solver used is NAGISA, which was developed by National Maritime Research Institute (Ohashi, Hino et al. 2019) and has been distributed to the maritime industry related companies and organizations in Japan. The code solves incompressible mass-conservation and Reynolds-averaged Navier-Stokes equations by structured grid based finite volume method. Velocity and pressure are coupled by artificial compressibility approach. Matrix system is solved using symmetric Gauss-Seidel method which is efficiently parallelized by the shared memory programming by OpenMP®. In the momentum and other transport equations, convective fluxes are evaluated by a 3rd-order upwind scheme based on flux-difference splitting, and diffusion fluxes are discretized by 2nd-order central differencing scheme. The 1st-order Euler backward scheme is utilized for temporal discretization, and steady state simulations are carried out.

The rotating propeller is modelled by simplified body force approach based on lifting line theory (Moriyama 1981). The body force distributions on a designated plane are calculated based on lifting line theory in which a propeller effect is represented by the vortices distributed on the panels tessellated on the propeller disk. The body force is distributed in cells with which a propeller disc intersects. There are two features of the present model are: 1) the effect of non-uniform propeller inflow can be considered and 2) the propeller open water characteristics (POC) is computed in the model and are not necessary to treat it as an input data when running the simulation with propeller effect.

Following, the computational settings for this research are detailed. The solver is capable of handling overset mesh with various topologies, but an OO-type mono mesh around hull is solely used. The outer boundary shape is a hemispherical ellipsoid with upper-lower symmetric boundary conditions applied by the assumption of a double-model flow. Especially in the towing condition, left-right symmetric boundary condition is additionally applied, simulations are conducted solely on the port-side region. Computational domain size is 8.0Lpp for forward and backward direction of the ship respectively, 6.0Lpp for downward and port/starboard-side direction, respectively.

As a turbulence model, explicit algebraic stress model based on k-omega base line formulation (EASM-BSL) is selected. To simulate boundary layer, the low Reynolds number model is applied, and all meshes are generated with the minimum grid spacing set to Y+= 0.5.

CNR-INM

Similarly to the “University of Genova”, CFD computations performed by CNR-INM have been carried out by using the open-source RANS solver OpenFOAM (V2306). Moreover, the widely used two-equation Shear-Stress Transport (SST) k-w has been adopted to model the effects of turbulence. A steady-state solver has been adopted with bounded second-order accurate schemes for all the transport equations. The computational meshes have been generated by means of the T-Rex approach within the Fidelity-Pointwise 2023 software. The T-Rex approach allows to generate prisms layers from the boundaries of unstructured domains (improving the quality of the mesh in the boundary layer region). For both the KCS and the JBC test cases, inlet and outlet

boundary conditions have been located at a distance of 1.5Lpp upstream and 3Lpp downstream the ship, respectively. The side and bottom boundaries, considered as slip walls, are located at 2Lpp far from the hull body. On the stern region, where the propeller takes place, further refinements have been considered. The total number of cells is about 3.8M and 5.6M for the JBC case at model and full scale, respectively; whereas, for the KCS a computational mesh counting of about 4.26M cells has been adopted for both the model and the full scale tests. The wall spacing for the model scale tests is less than 100 viscous units for both ship model; whereas, for the full scale tests y^+ is about 100 and 5000 on the average for the JBC and the KCS model, respectively.

UoS / ShortCut CFD

The computations are performed using the OpenFOAM CFD suite together with the SHORTCUt package (Winden 2021) for pre-processing and self-propulsion modelling. The potential flow solver used is the standard OpenFOAM solver potentialFoam, based on implicitly solving the Laplace equation. The RANS solver used is based on the standard simpleFoam solver from OpenFOAM, modified to include a body force model for the propeller. This solver is steady state and based on the SIMPLE pressure-velocity coupling algorithm. These simulations are part of a larger dataset, previously published by Andersson, Shiri et al (2022).

The domain considered is a rectangular basin with the hull forward perpendicular located 1Lpp downstream of the inlet and extending 5Lpp behind the aft perpendicular. The total width of the domain is 2Lpp and the total length is 7Lpp. A double model approach is used where the waterline is considered as a symmetry plane. The depth of the domain is 1.5Lpp. The rudder is included in the simulations. No other appendages are considered.

The mesh is unstructured and hex-dominant, with prism layers added near the hull for resolving the boundary layer. The near-hull mesh is designed to satisfy y1+= 100 in full scale and y1+< 1 in model scale and the surface mesh on the hull was designed to keep the aspect ratio of the first cell below 1500. As a result, the total mesh size is large; owing to the high Reynolds number of the full scale case. The cell size on the hull surface is approximately 0.00070Lpp. There is extra refinement on the stern near the propeller, as well as the propeller wake, to a size of around 0.00018Lpp. The total mesh size is 36.4M cells. The same mesh is used for both full- and model scale calculations as well as for the potential flow solution.

The Menter SST model is used for turbulence modelling. For the full scale case where y1+>1, wall functions are applied, including allowance for hull roughness as suggested by Sakamoto, Kobayashi et al. (2020). The grain roughness on the hull is set to 100 micrometers and the turbulence intensity at the inlet is set to 1%.

In this study, the SHORTCUt framework is used to couple the OpenFOAM RANS solver (simpleFoam) with the Yamazaki simplified propeller theory (Yamazaki 1998). RPM and body force distribution are updated iteratively to find the full scale self-propulsion point every 50 iterations of the main flow solver. The Yamazaki theory allows for deduction of the propeller induced velocities, and therefore a separation of the effective- and total wakes.
A total of 2000 SIMPLE iterations are conducted for the RANS resistance test and a further 1500 iterations are conducted for the coupled RANS-Yamazaki self-propulsion test.

UM

The steady RANS double solution is computed using the software HELYX, which is provided by Engys. The solution for the ONR Tumblehome and the KVLCC2 are provided for analysis. The computational meshes are generated with helyxHexMesh, which is part of helyx. The mesh is hex-dominant but body fitted with local refinement around fine features of the hull and flow solution. Boundary layer prisms are used on the wall surfaces, with an average y+ of 35 on the hull surfaces at model scale, and approximately 1000 at full scale. A wall function is used with the k-omega SST turbulence model.

DUT

The simulation employed the standard "Yupeng" model, and the 1:26.8 scale model underwent drag resistance experiments at the towing tank. Subsequently, this studyexplored various scale ratios based on the results from the experiments.

The simulation software employed was STARCCM+, utilizing the SST K-Omega turbulence model with wall-distance. To ensure minimal interference with the results, identical CPU cores were utilized. The simulation adopted a "stacking model" approach, symmetrically treating the ship model at the draft waterline according to its posture during towing tank

experiments. This approach allows for disregarding the air and free surface components above the draft waterline in order to reduce computational resource consumption by avoiding increased grid size at the free surface position. However, this method neglects the effects of free surfaces and does not account for resistance caused by wave-making at the bow and stern during ship navigation simulations. Additionally, propellers are excluded from half of the ship in this simulation. According to the boundary layer theory and software requirements, the Wall Y+ is controlled at approximately 100. While simulating different scale ratios, the same grid division form is adopted; however, as the scale ratio decreases, the number of grids increases due to changes in boundary layer thickness. A smaller scale ratio necessitates a thinner boundary layer, thus requiring more grids.

To reduce grid demands, a symmetrical method is employed for nominal wake calculation by considering only the right half of the ship. The propeller disk surface serves as the location for monitoring wake field with calculation points ranging from 0.2 to 1.1 times of the propeller's radius for wake fraction determination. A total of 370 monitored points are set at intervals of 5° from 180° to 360°.For working conditions involving a propeller, a virtual disk method is utilized. Since it is not possible to track the internal area of this virtual disk accurately, time-lapse wake monitoring position is set at a plane located at approximately 0.3 times of the propeller radius in front of its disk. This calculation monitors points every 5° within a range from 0° to 360° with radii varying between 0.2 and 1.1 times.

CSSRC

CSSRC uses the XCHAP solver from the commercial software SHIPFLOW for the computations of JBC and KCS. XCHAP is a finite volume code that solves the Reynolds averaged Navier-Stokes equations on overlapping, structured grids. It uses several turbulence models (EASM, k-ω BSL, k-ω SST). In the present work, the EASM (Explicit Algebraic Stress Model) turbulence model which is the most advanced model is employed in the viscous flow simulation. This model takes into account the non-linear terms as well. The control equation is dispersed by the finite volume method. The convective terms are discretized with a Roe scheme and a second order explicit defect correction is used to approach second order accuracy. The rest of the terms are discretized with central differences. A local artificial time-step is added to the equations and the discrete coupled equations are solved using an ADI-solver.

The potential wake fields are computed using the panel code module XPAN of SHIPFLOW. The effective wake fields are determined with the RANS-LL (lifting line) coupling approach provided by SHIPFLOW. In the lifting line model, a finite-bladed propeller is first replaced with an infinite-bladed propeller. A series of distributed vortex systems are then used to represent the propeller. The slipstream contraction is not considered in this model because the pitch and the radius of each vortex line are assumed to be constant. Only the steady part of induced tangential and axial velocity is taken into account. For the RANS-LL coupling, the propeller is modelled as an actuator disc and the effects of the propeller are introduced as body forces for numerical modelling in the RANS simulation. By applying the body forces to discretized cells on the propeller disc, the flow is accelerated in the same way as suction of the flow by the propeller. The velocity computed by the RANS solver over the whole domain, subtracting the induced velocity estimated by the LL method leads to the effective wake.

Structured H-O type computation grids are generated automatically with the solver module XGRID of the SHIPFLOW software. The grids extend from -1.0 L_{PP} (upstream boundary) to 3.0 L_{PP} (downstream boundary) in the longitudinal direction and has a radial section of 3.0 L_{PP}. The propeller is modelled by cylindrical grid with the overlapping grid technique on the top of back ground grid for hull geometry. No wall functions are used in the code. The total number of cells is around 9.4 M for JBC and KCS at both model scale and full scale. The y+ in both cases is below 1 for the model scale and ranges between 1 and 300 for the full scale.

UNCERTAINTY ASSESSMENT

Numerical uncertainties of the CFD predictions are assessed by following the ITTC Recommended Procedures and Guidelines (RP) 7.5-03-03-01 (ITTC 2021). The methodology is solution Verification, Validation, and Uncertainty Assessment (VVUA) to quantify numerical and modelling errors. Solution verification is to estimate the numerical errors due to the mesh discretization, numerical iteration, and other parameters used in the simulation. Validation is to assess the modelling errors by comparing the computational simulation results with experimental data. Herein, solution verification considers only the mesh discretization, and validation is not performed due to the lack of experimental data available. Uncertainty assessment uses the Least Squares Root (LSR) approach presented in RP 7.5-03-01-01. Any

point or integral variable of the simulation ϕ is curve-fitted by using an error estimator ϵ_ϕ and the uncertainty is determined as

$$U_\phi = \begin{cases} F_S\epsilon_\phi + \sigma + |\phi - \phi_{fit}|, & \sigma < \Delta_\phi \\ 3\frac{\sigma}{\Delta_\phi}(\epsilon_\phi + \sigma + |\phi - \phi_{fit}|), & \sigma \geq \Delta_\phi \end{cases} \quad (1)$$

Here, ϕ_{fit} is the curve fit of ϕ, F_S is a safety factor chosen based on the goodness of the curve fit, σ is the standard deviation for the curve fit with respect to ϕ, Δ_ϕ is a data range parameter. Eça and Hoekstra (2014) provide the full definitions and more details of the procedure.

Table 2 summarizes the grid information of the present VVUA for five different simulation cases, where n_g is the number of considered grids and N_1 is the cell count of the finest grid. For the use of LSR approach, $n_g \geq 4$ for all the cases are needed. Appendix A shows the solution convergence with the grid refinement.

Table 3 presents the resulting uncertainties of the model wake U_{w_m}, full-scale wake U_{w_s}, potential wake U_{w_p}, and the model- and full-scale friction coefficients $U_{C_{fm}}$ and $U_{C_{fs}}$. In addition, the uncertainties of the following two derived variables are also considered, which are the ratio of friction wake, w_f^*, and the ratio of friction coefficient, C_F^*, between the model- and full-scale, each defined as

$$w_f^* = \frac{w_m - w_p}{w_s - w_p} \quad (2)$$

$$C_F^* = \frac{C_{Fm}}{C_{Fs}} \quad (3)$$

The uncertainties of the above two variables are estimated by propagating the uncertainties of the elemental variables. In general, the uncertainties in the wake variables U_{w_m}, U_{w_s}, and U_{w_p} are within 1~5% except for Case 5, and those in the friction coefficients $U_{C_{Fm}}$ and $U_{C_{Fs}}$ are also 1~5% for all the cases. The uncertainties in the friction wake ratio $U_{w_f^*}$ is relatively high, 5~15%, again except for Case 5, whereas the uncertainty in the friction coefficient ratio $U_{C_F^*}$ is relatively low, 0~4% for all the cases.

For Case 5, a careful interpretation is required for the uncertainty values of the wake variables shown in Table 3. The ONRT hull form used for this case is a twin-screw ship with an open-shaft type stern and is characterised by a very small wake fraction of an order smaller magnitude (~0.02), which made the relative (or the percentage) uncertainty values seem large. This fact is even more evident from seeing the absolute uncertainty values are comparable with those for the other simulation cases as shown in Table B1 of Appendix B. Thus, it can be justified to consider the computational outcomes of Case 5 are of equal quality as those of the other simulation cases and the conclusions reported in the subsequent sections can be considered valid.

Table 2. Grid information for VVUA.

Case No.	Institute	Hull Form	n_g	N_1
1	MARIN	KCS	7	9,472,000
2	UNIGE	KCS	6	12,444,794
3	SRCJ	JBC	4	25,747,728
4	UM	KVLCC2	6	77,634,253
5	UM	ONRT	6	34,884,580

Table 3. VVUA results.

Case No.	U_{w_m} (%)	U_{w_s} (%)	U_{w_p} (%)	$U_{C_{Fm}}$ (%)	$U_{C_{Fs}}$ (%)	$U_{w_f^*}$ (%)	$U_{C_F^*}$ (%)
1	1.6	1.4	0.5	0.3	0.3	4.6	0.3
2	4.8	2.4	3.6	4.2	0.5	12.8	2.3
3	1.2	2.6	0.1	0.8	0.9	6.8	0.9
4	2.4	3.6	1.3	5.2	3.5	11.9	4.3
5	3.1	12.6	12.7	4.6	2.8	80.4	3.5

RESULTS

In the report of the Performance Committee of the 15th ITTC (1978) the section on the wake fraction states: "*... there has been no practical alternative to the Tanaka-Sasajima method which is based on the assumption that there is a linear relation between the wake fraction and the frictional (viscous) resistance coefficient*". This refers to the contribution of Sasajima and Tanaka in the report of the Performance Committee of the 11th ITTC (1966) where the wake fraction is decomposed in a potential component, w_p, and a frictional component, w_f.

$$w = w_p + w_f \quad (4)$$

Similarly, although not explicitly stated in their paper, the thrust deduction, t, is decomposed in a potential component and a frictional component.

$$t = t_p + t_f \quad (5)$$

Referring to Fresenius, Dickmann and many other publications, they suggested that the potential part of

the wake fraction is proportional to the potential part of the thrust deduction:

$$t_p = \alpha_p w_p \qquad (6)$$

In the next two sections potential wakes will be presented that have been computed using CFD for a number of ships. For those cases where power predictions have been performed in inviscid flow, thrust deduction fractions have been determined as well. These are used to verify to what extent CFD methods confirm the validity of eq. (6).

Potential part of the wake fraction

Replacing the no-slip boundary condition at the wall by a free-slip boundary condition, CFD codes that are generally used to compute viscous flow can be used to compute inviscid flow solutions. Alternatively, without replacing the no-slip boundary condition, the potential wake in the propeller plane can be obtained by performing the computation sailing in reverse direction. This approach mimics early experimental work where the potential wake was measured while towing backwards. In the present study SRCJ has determined potential wakes using this approach.

From the solutions the axial velocity distribution at the propeller reference plane has been interpolated and at the left-hand side of Figure 1 through Figure 5 the potential axial wake fields are shown for the ONRT, KCS, YUPENG, JBC and KVLCC2, respectively. In the middle of these figures the corresponding full-scale wakes are shown and on the right the model scale axial wake fields. The potential wakes show a clear difference between the various cases, with higher potential wake fractions for the full-blocks ships (KVLCC2 and JBC) compared to the more slender container ships (KCS and YUPENG). This is in line with what is well-known for the viscous wake fields of these ships.

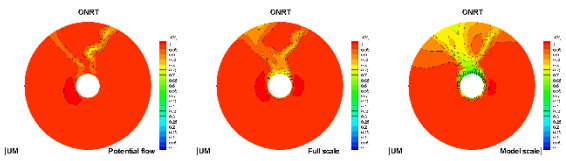

Figure 1 ONRT potential (left), full scale (middle) and model scale (right) axial wake fields.

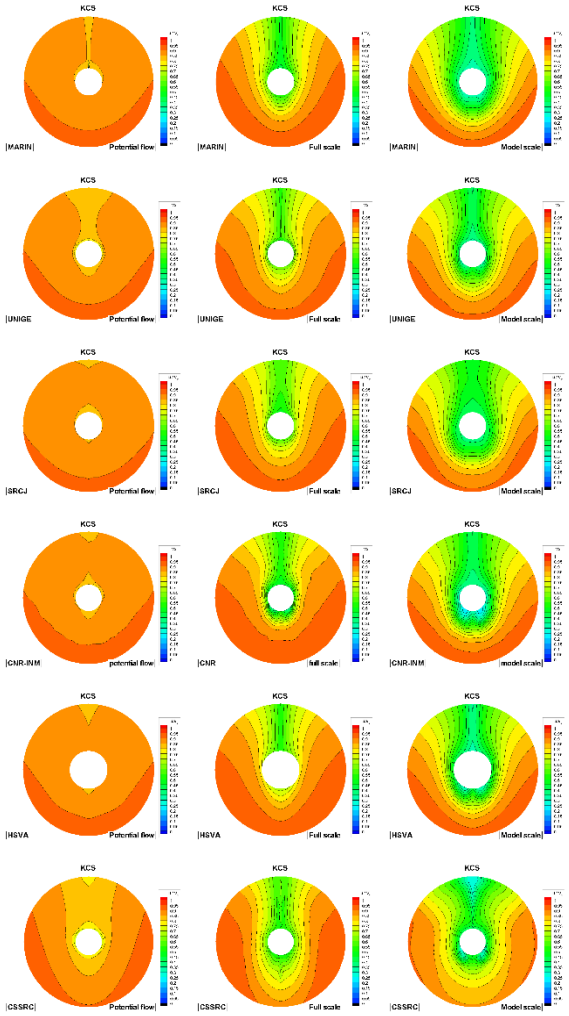

Figure 2 KCS potential (left), full scale (middle) and model scale (right) axial wake fields.

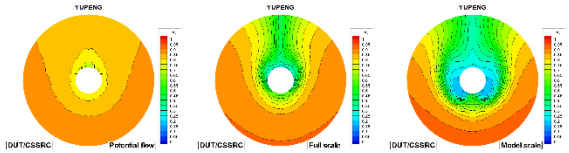

Figure 3 YUPENG potential (left), full scale (middle) and model scale (right) axial wake fields.

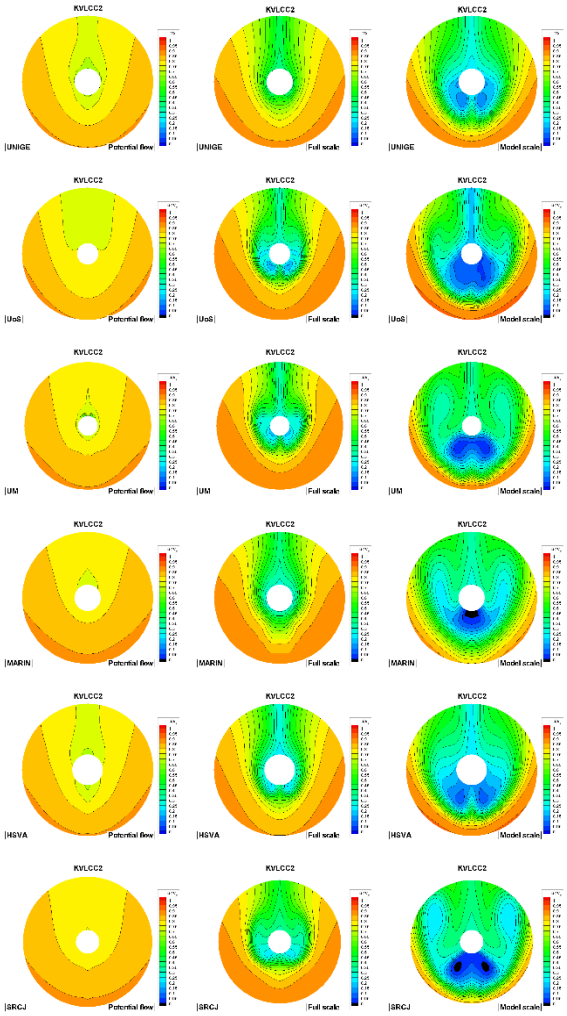

Figure 4 KVLCC2 potential (left), full scale (middle) and model scale (right) axial wake fields.

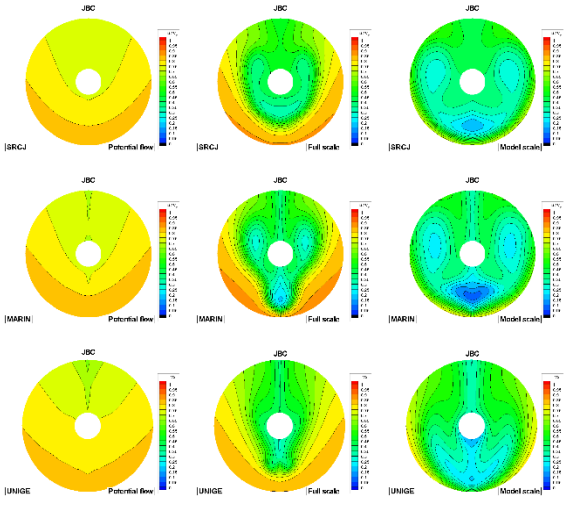

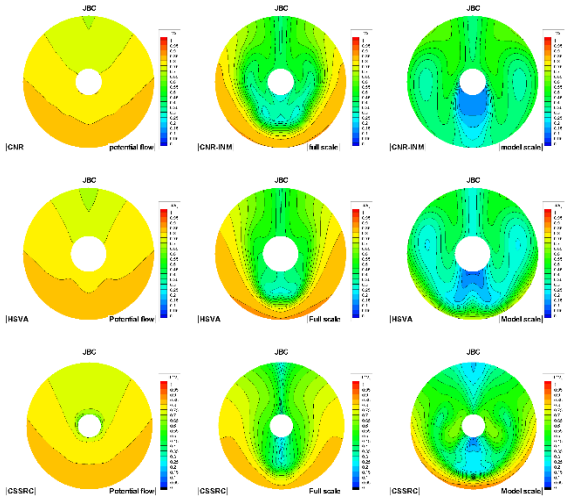

Figure 5 JBC potential (left), full scale (middle) and model scale (right) axial wake fields.

Potential, full-scale and model-scale wake fractions that have been integrated from these fields are listed in Table 4 through Table 6. In all cases the potential wake is smaller than the full-scale wake, and the full-scale wake in its turn smaller than the model-scale wake. The mean potential wake fraction of the most slender ship (the KCS) is just below half the mean value the model-scale wake fraction, and thus the viscous part and the potential part of the wake fraction are approximately equal for this case. The magnitude of viscous effects are larger for the KVLCC2 and the JBC, both considerably fuller hull forms, and for those cases the viscous part of the wake is more than twice as large as the potential part of the wake. And it can be observed that the standard deviation in the wake fractions as predicted by the various participants is smallest for the potential wake and largest for the model-scale wake.

Table 4: Potential-wake fractions of the three cases analyzed by multiple participants.

	KCS	KVLCC2	JBC
MARIN	0.119	0.190	0.230
UniGe	0.121	0.207	0.231
SRCJ	0.120	0.185	0.232
CNR-INM	0.116	-	0.229
UoS	-	0.218	-
UM	-	0.193	-
HSVA	0.114	0.204	0.221
CSSRC	0.126	-	0.230
mean	0.119	0.200	0.229
stdev	0.004	0.012	0.004

Table 5: Full-scale nominal wake fractions of the three cases analyzed by multiple participants.

	KCS	KVLCC2	JBC
MARIN	0.187		0.407
UniGe	0.173	0.262	0.345
SRCJ	0.173	0.284	0.383
CNR-INM	0.175	-	0.404
UoS	-	0.325	-
UM	-	0.287	-
HSVA	0.162	0.311	0.357
CSSRC	0.180	-	0.382
mean	0.175	0.294	0.380
stdev	0.008	0.025	0.025

Table 6: Model-scale nominal wake fractions of the three cases analyzed by multiple participants.

	KCS	KVLCC2	JBC
MARIN	0.298	0.534	0.630
UniGe	0.250	0.426	0.541
SRCJ	0.257	0.544	0.605
CNR-INM	0.270	-	0.600
UoS	-	0.539	-
UM	-	0.528	-
HSVA	0.258	0.550	0.634
CSSRC	0.303	-	0.595
mean	0.273	0.520	0.601
stdev	0.023	0.047	0.033

Potential part of the thrust deduction

To determine the potential part of the thrust deduction, propulsion computations have been performed in inviscid flow. In these computations (performed by UniGe, CNR-INM and MARIN) the imposed thrust was set equal to the thrust in the corresponding propulsion computation for viscous flow. In the RANS-BEM computations by MARIN, the propeller rotation rate was iterated to obtain the required thrust.

In double-body CFD computations the resistance in inviscid-flow computations should be small and vanish with grid refinement. Any non-zero resistance value can be considered a measure for the remaining discretization or iterative error in the CFD computation. As a similar error is likely to be present in corresponding propulsion computations these errors may (partly) cancel when computing the thrust deduction. However, in the present study this issue is not further considered.
A consequence of having zero resistance in an inviscid double-body computation is that the resistance force acting on the hull in the corresponding propulsion computation is solely caused by the pressure decrease at the stern due to propeller action.

Figure 6 presents the inviscid-flow thrust deductions, evaluated as: $t_p = (R_T^* - R)/T$. Here R is the resistance in a nominal-wake computation, T the imposed thrust and R_T^* the resistance force acting on the hull in a propulsion computation. The predicted potential thrust deduction increases with increasing potential wake fraction, confirming the assumed proportionality formulated in eq. (6) albeit with substantial scatter around the line $t_p=w_p$. The (Pearson) correlation coefficient (r) that is a measure of the strength of the linear association between the two variables is equal to r=0.939.

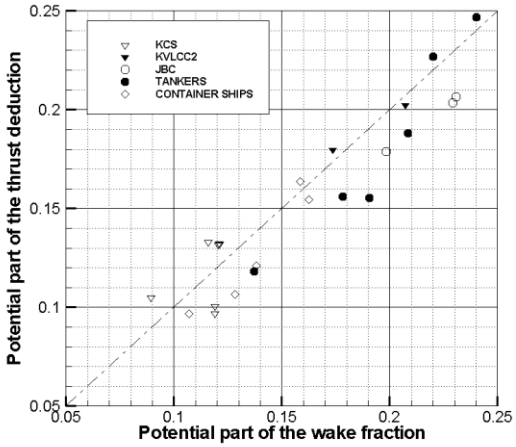

Figure 6 Relation between the potential part of the nominal wake fraction and the thrust deduction.

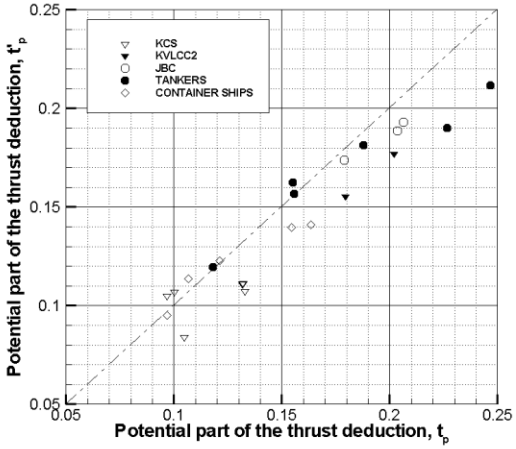

Figure 7 Relation between the potential part of the thrust deduction and the thrust deduction according to eq. (7).

Already in early papers it was reported that a more generally valid relation between the potential part of

the thrust deduction and the wake fraction could be obtained by the expression

$$t'_p = 2w_p/(1+sqrt(1+C_{th})) \quad (7)$$

Here C_{th} is a thrust coefficient based on the propeller diameter: $C_{th} = T/(1/2\ \rho\ \pi/4\ D^2)$, which can also be rewritten as $C_{th} = 8K_T/\pi J^2$. Comparing eq. (7) with the CFD-predicted thrust deductions, see Figure 7, in general lower values are found in the CFD, especially at higher thrust deduction. The (Pearson) correlation coefficient is equal to r=0.932. Thus it is concluded that the assumption that the potential part of the wake fraction is proportional to the potential part of the thrust deduction is reasonably well-supported by the present inviscid-flow results.

Scale effect on the frictional part of the thrust deduction

The second assumption mentioned in the Sasajima-Tanaka paper is that the scale effect on the frictional part of the thrust deduction is small. To verify this assumption, the thrust deduction from the potential-flow solutions is subtracted from the corresponding model and full-scale viscous-flow solutions, and the result is shown in Figure 8.

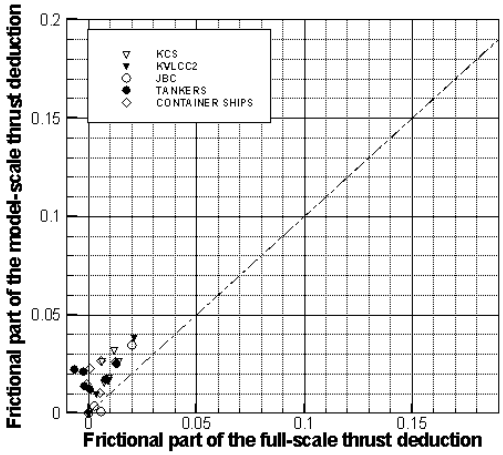

Figure 8 Scale effect on the frictional part of the thrust deduction.

The CFD computations indicate that the scale effect on the frictional component of the thrust deduction is *not* necessarily small; with only one exception the values at model scale are higher than at full scale and increasingly so with increasing thrust deduction. On the other hand the magnitude of the frictional part of the thrust deduction is considerably smaller than the potential part of the thrust deduction that ranges between $0.10 < t_p < 0.25$ both at model and at full scale.

It is concluded that even if the scale effect on the frictional part of the thrust deduction is not small, it is not likely to be an important assumption in the Sasajima-Tanaka procedure. The relation $w_p=t/\alpha$ can still be regarded as a reasonable approximation provided the parameter α is allowed to vary between full scale, model scale (and potential flow), see Figure 9. In the original paper it was tentatively put to unity. For the model and full-scale thrust deduction the (Pearson) correlation coefficient are equal to r=0.907 and r=0.900, respectively. Thus

$$t_p = \alpha_p\ w_p \quad (8a)$$

$$t_s = \alpha_s\ w_p \quad (8b)$$

$$t_m = \alpha_m\ w_p \quad (8c)$$

and so $w_p = t_p/\alpha_p = t_s/\alpha_s = t_m/\alpha_m$.

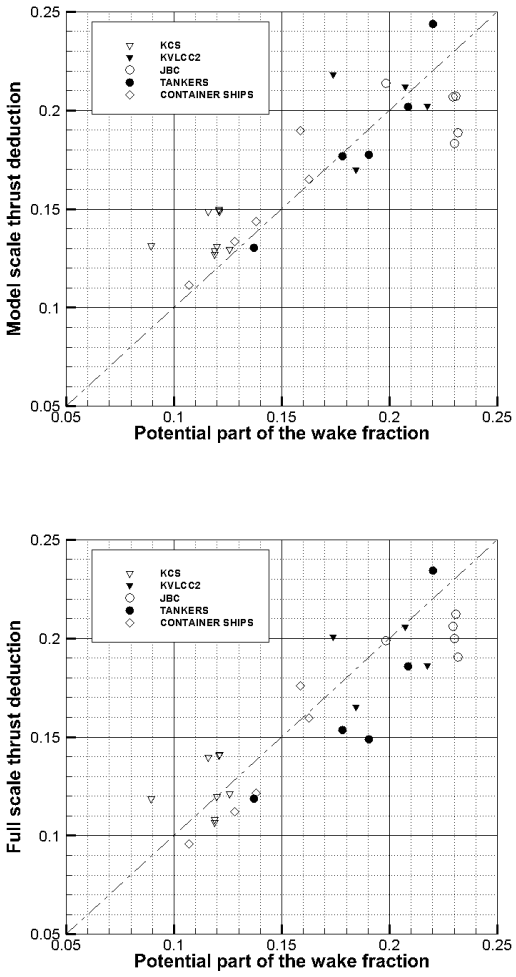

Figure 9 Predicted relation between wake fraction and thrust deduction. Top: model scale, bottom: full scale.

Scale effect on the wake fraction

Shifting the viscous part of the wake fraction to the left-hand side of the equation and using equation (8a) to eliminate the potential part of the wake fraction gives

$$w_{fs} = w_s - w_p = w_s - t_s/\alpha_s = w_s - t_m/\alpha_m$$

$$w_{fm} = w_m - w_p = w_m - t_m/\alpha_m$$

Division of these two expressions yields

$$w_{fs}/w_{fm} = (w_s - t_m/\alpha_m)/(w_m - t_m/\alpha_m)$$

Now re-ordering so that an expression for the full-scale wake fraction is obtained, gives

$$w_s = t_m/\alpha_m + (w_m - t_m/\alpha_m)\, w_{fs}/w_{fm} \qquad (9)$$

The final approximation in the paper by Sasajima and Tanaka is that the scale effect on the wake fraction, w_{fm}/w_{fs}, is principally determined by a function of C_{Fm}/C_{Fs}. From a fit through their data, that according to themselves excludes 'extremely' full ships, they proposed

$$w_{fm}/w_{fs} = C_{Fm}/C_{Fs} \qquad (10)$$

The ratio of the friction coefficients was tentatively taken as 1.8 by them, compared to $1.8 < C_{fm}/C_{fs} < 2.2$ in the present CFD results. This range agrees well with the ratio that follows from various plate-friction lines, as shown in Figure 10 where the symbols indicate the Reynolds numbers in the viscous-flow predictions of the present test cases.

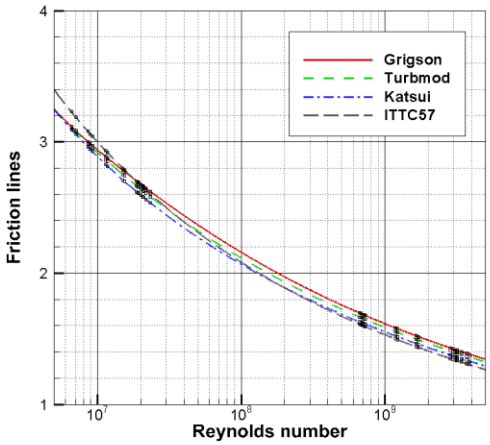

Figure 10 Scale effect on the friction coefficient according to various friction lines.

Figure 11 compares the CFD predicted friction ratios against the CFD predicted ratio of the frictional part of the wake fractions at model and full scale. From these it is clear that the present results do not support the assumption formulated in eq. (10) at all. The variation in the wake scale effect that follows from the viscous flow computation is much larger than assumed in the Sasajima-Tanaka method.

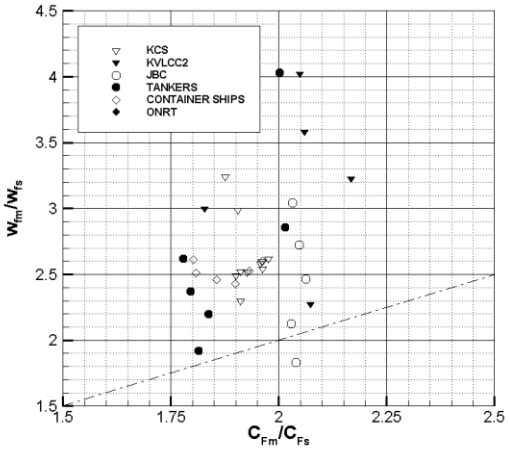

Figure 11 CFD prediction of the relation between the scale effect on the frictional part of the *nominal* wake fraction and the scale effect on the friction coefficient.

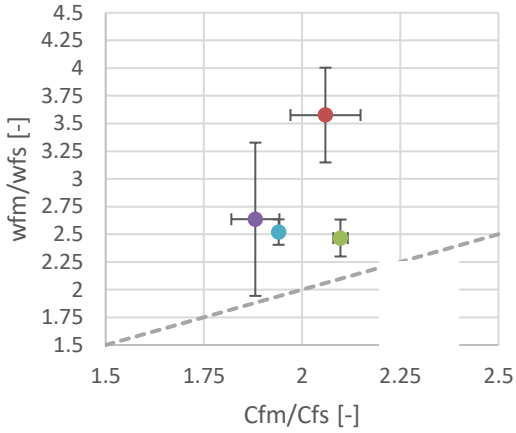

Figure 12 Uncertainty quantification applied to the scale effect on the frictional part of the *nominal* wake fraction and the scale effect on the friction coefficient.

For four of these cases simulations have been finished at a sufficient number of grids to perform uncertainty quantification. This is shown in Fig. 12. The cases are the KCS by MARIN (blue dot) and by UniGe (purple dot), the JBC by SRCJ (green dot), the KVLCC2 by

UM (red dot). Little uncertainty is found for friction ratio. The uncertainties are higher for the wake fraction ratios, especially for KCS by UniGe, but the VVUQ procedure supports the conclusion that the scale effect on the frictional part of the wake fraction varies between the cases.

In the ITTC "78 proceedings it was already stated that the assumed linear relation between the wake fraction and the frictional (viscous) resistance coefficient could not be physically correct but that the method gave acceptable results when the *effective* wake was used instead of the nominal wake. Therefore a number of cases have been simulated including propeller action, both at model and full-scale Reynolds number and for potential flow. From these effective wake fractions have been determined. The thrust in a potential-flow computation has been taken equal to the thrust in the corresponding viscous-flow computation. The results are shown in Figure 13.
Compared to Figure 11 the spreading in vertical direction has indeed been reduced and results for the same test case (e.g. KCS) are grouped closer together. However, also when using the effective wake the conclusion remains that the assumption that the scale effect on the wake fraction, w_{fm}/w_{fs}, is principally determined by a function of C_{Fm}/C_{Fs} is not supported by the CFD computations.

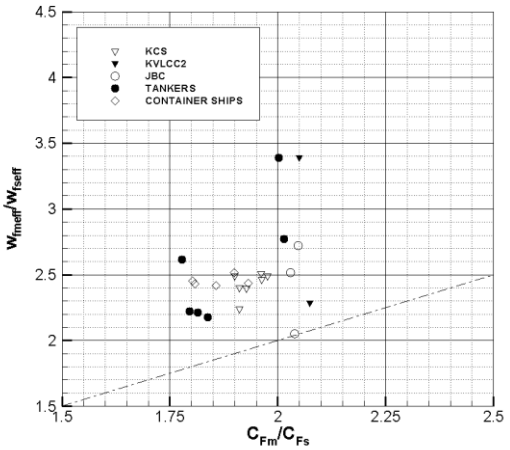

Figure 13 CFD prediction of the relation between the scale effect on the viscous part of the *effective* wake fraction and the scale effect on the friction coefficient.

Sasajima-Tanaka wake scaling

Substitution of eq. (10) in eq. (9) results in a linear relation between the wake fraction and the friction resistance:

$$w_s = t_m/\alpha_m + (w_m - t_m/\alpha_m)\, C_{Fs}/C_{Fm} \qquad (11)$$

and substituting α_m=1 results in the Sasajima-Tanaka formula

$$w_s = t_m + (w_m - t_m)\, C_{Fs}/C_{Fm} \qquad (12)$$

The first term on the right-hand side in eq. (12) corresponds to the potential part of the wake fraction and the second term on the right-hand side to the viscous part of the wake fraction. A check of the cumulative effect of the three assumptions underlying the Sasajima-Tanaka formula can be obtained by substituting the values of t_m, w_m, C_{Fs} and C_{Fm} from the CFD computations in eq. (12) and comparing the resulting approximated full scale wake fraction with the value coming directly from the CFD computations. This is shown in Figure 14. Consistent with the earlier results evaluation of the Sasajima-Tanaka formula using CFD input results in higher approximated values for the ship wake fraction than directly obtained from the full-scale simulations.

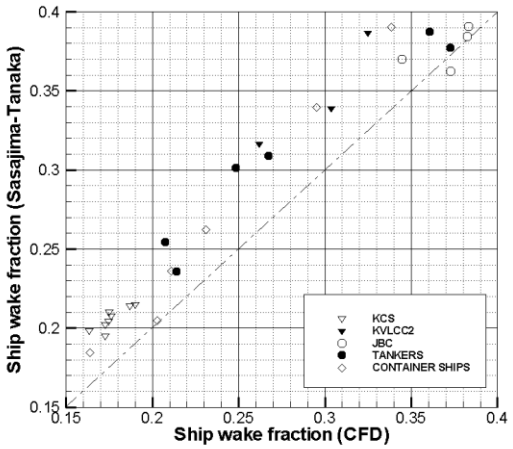

Figure 14 Comparison between the CFD predicted *nominal* ship wake fraction and the Sasajima-Tanaka method.

ITTC78 wake scaling

There are a few differences between eq. (12) and the ITTC78 wake scaling formula given by

$$w_{TS} = (t + w_R) + (w_{TM} - t - w_R)\frac{(1+k)C_{FS} + \Delta C_F}{(1+k)C_{FM}} \qquad (13)$$

First of all in the ITTC78 formula the effective (or Taylor) wake fractions are used instead of the nominal wake fractions. Experimentally, the effective wake

fraction is typically determined from propulsion measurements at self-propulsion point in combination with open-water propeller diagrams. Secondly, friction lines or specifically the ITTC57 model-ship correlation line are used to estimate the friction resistance coefficients at model and full scale. On top of that two additional contributions for the effect of the rudder on the wake fraction and the surface roughness on the full scale friction resistance are added to the ITTC78 formula. Similar to eq. (12) the first term on the right-hand side of the ITTC78 formula corresponds to the potential part of the (effective) wake fraction. The second term on the right-hand side consists of the sum of the viscous part of the effective wake fraction and a full-scale roughness contribution. All three parts are crucial for considering the full-scale effective wake, but to proceed cautiously in a step-by-step manner, this investigation is limited to the first two parts: the dominant factors in wake scaling.

When comparing the full-scale effective wake fractions following from the full-scale CFD computations with the values that are obtained by evaluating the ITTC78 formula using model-scale CFD data, the result shown in Figure 15 is obtained. Here it can be seen that direct CFD prediction of the effective wake fraction gives consistently lower values than the extrapolation of the model scale CFD using the ITTC78 formula.

The right-hand side of Figure 16 shows a similar result when using the Yazaki method The results indicate consistency between the methods and give confidence that RANS-based CFD methods can be used as an alternative to more traditional empirical formulae to determine the full-scale effective wake.

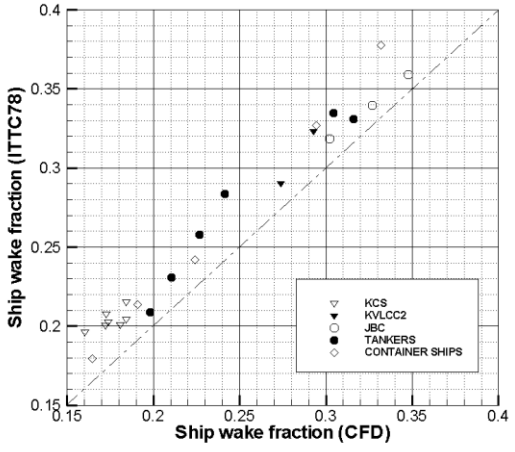

Figure 15 Comparison between the CFD predicted ship wake fraction and ITTC78 formula with model-scale CFD input.

Yazaki method

In the Yazaki method, a diagram is used to estimate the scale effect of the effective wake fraction from the model tank test. While considering the theoretical background of scale effects, the diagram was created by analysing many sea trial results and towing tank results. Main factors used in the diagram as the index to estimate the scale effect are L_{PP}, $1\text{-}w_{TM}$ and B/T_A. The diagram can directly demonstrate *ei* value which includes scale effect and roughness effect. Here, *ei* is the ratio of $1\text{-}w_{TS}$ to $1\text{-}w_{TM}$, as represented in eq. (14).

$$ei = (1\text{-}w_{TS}) / (1\text{-}w_{TM}) \quad (14)$$

The applicable vessels are single-screw and single-rudder ships with a L_{PP} ranging from 80m to 400m and a B/T_A ratio within the range of 2.0 to 6.0.

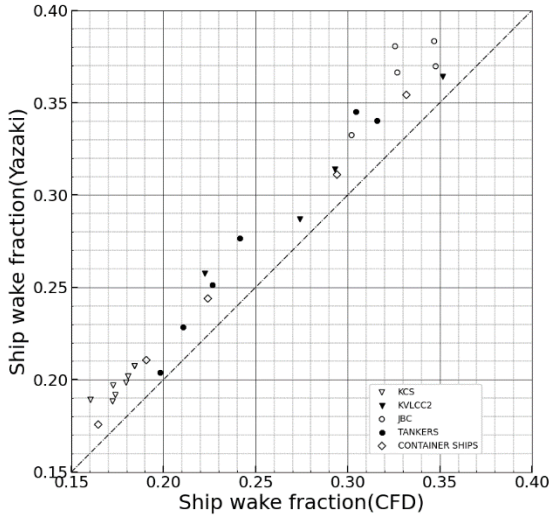

Figure 16 Comparison of the CFD prediction of the full-scale effective wake fraction with the Yazaki method, using model-scale CFD input.

CONCLUSION

With respect to the assumptions underlying wake scaling procedures it is concluded that:

According to the CFD, the potential part of the wake fraction is indeed proportional to the potential part of the thrust deduction.

According to the CFD, the scale effect on the frictional part of the thrust deduction is not necessarily small. However, the frictional part is small compared to the potential part of the thrust deduction, it may not be an important assumption, and thus may introduce a relatively small error in the extrapolation procedure.

The CFD does not at all support the assumption that the scale effect on the wake fraction is principally determined by a function of the scale effect on the friction coefficient: there is a large variation in predicted model-to-ship wake-fraction ratios between the various test cases.

Simplifications in the present CFD results will have some effect on the final wake scaling, and thus require further attention. Nevertheless, from this study it is concluded that improvements in extrapolation procedures can be obtained, especially by replacing the assumed linear relation between the scale effect on the friction coefficient and the scale effect on the wake fraction with a CFD-based procedure.

REFERENCES

Andersson, J., et al. (2022). "Ship-scale CFD benchmark study of a pre-swirl duct on KVLCC2." Applied Ocean Research 123: 103134.

Bruzzone, D., et al. (2014). Rudder-propeller interaction: analysis of different approximation techniques. Proceedings of the 11th international conference on hydrodynamics ICHD.

Dickmann, H.E., 1939, "Wechselwirkung zwischen Propeller und Schiff unter besonderer Berücksichtigung des Welleneinflusses", Jahrbuch der Schiffbautechnischen Gesellschaft

Eça, L. and M. Hoekstra (2014). "A procedure for the estimation of the numerical uncertainty of CFD calculations based on grid refinement studies." Journal of computational physics 262: 104-130.

Fu, T.C. et al, "Final Report and Recommendations of the Specialist Committee on Scaling of Wake Field" Proceedings of the 26th ITTC Conference. 2011.

ITTC, (1978). "Performance Prediction Method," ITTC Recommended Procedures and Guidelines 7.5-02-03-01.4, Revision 04

ITTC, 2021, "Uncertainty Analysis in CFD, Verification and Validation Methodology and Procedures," ITTC Procedure 7.5-03-01-01, Revision 04.

Moriyama, F. (1981). "On the effect of a rudder on propulsive performance." Journal of the Society of Naval Architects of Japan 1981(150): 63-73.

Ohashi, K., et al. (2019). "Development of a structured overset Navier–Stokes solver with a moving grid and full multigrid method." Journal of Marine Science and Technology 24: 884-901.

Sakamoto, N., et al. (2020). "An overset RaNS prediction and validation of full scale stern wake for 1,600 TEU container ship and 63,000 DWT bulk carrier with an energy saving device." Applied Ocean Research 105: 102417.

Sasajima, H. and Tanaka, I., "On the estimation of wake of ships," Proceedings of the 11th ITTC Conference, 1966, pp. 140-143.

Villa, D., et al. (2019). "An efficient and robust approach to predict ship self-propulsion coefficients." Applied Ocean Research 92: 101862.

Winden, B. (2021). "An open-source framework for ship performance CFD". SNAME Offshore Symposium, SNAME.

Yamazaki, R. (1998). "Deduction of the Simplified Propeller Theory". Transactions of the West-Japan Society of Naval Architects (西部造船会会報), 95 p251-271

Yazaki, A. (1969). "A diagram to estimate the wake fraction for an actual ship from model tank test". Proceedings of the 12th International Towing Tank Conference, Rome, Italy.

APPENDIX A: Solution Convergence

Figure A1 shows the convergence of model wake w_m, full-scale wake w_s, and potential wake w_p, and Figure A2 shows those of the model- and full-scale friction coefficients, C_{Fm} and C_{Fs}, respectively, with respect to the grid size change. In these figures, grid size is presented with a grid refinement ratio defined as

$$r_i = \sqrt[3]{N_1/N_i} \tag{A1}$$

The index i = 1, …, n_g indicates each grid case, N_i is the cell counts of the grid, and n_g is the total number of grid cases.

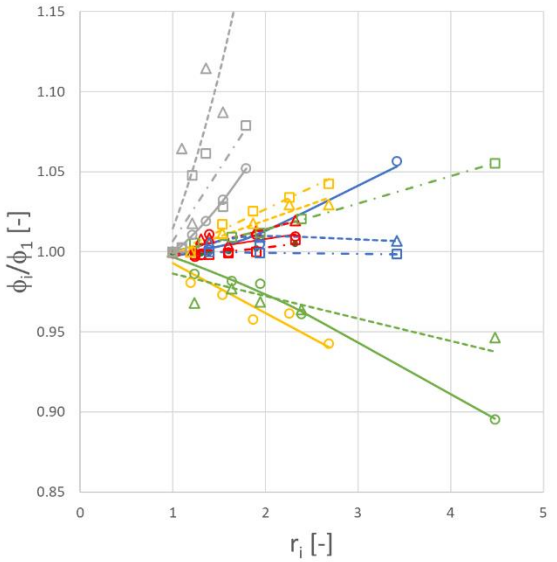

Figure A1. Relative solution convergence with the grid refinement ratio for $\boldsymbol{\phi} = \boldsymbol{w_m}$(circle), $\boldsymbol{w_s}$ (triangle), and $\boldsymbol{w_p}$ (square), and $\boldsymbol{\phi_{fit}} = \boldsymbol{w_m}$ (solid line), $\boldsymbol{w_s}$ (dashed line), and $\boldsymbol{w_p}$ (dash-dot line) of VVUA Case No. 1 (red) , 2 (yellow), 3 (blue), 4 (green), and 5 (gray).

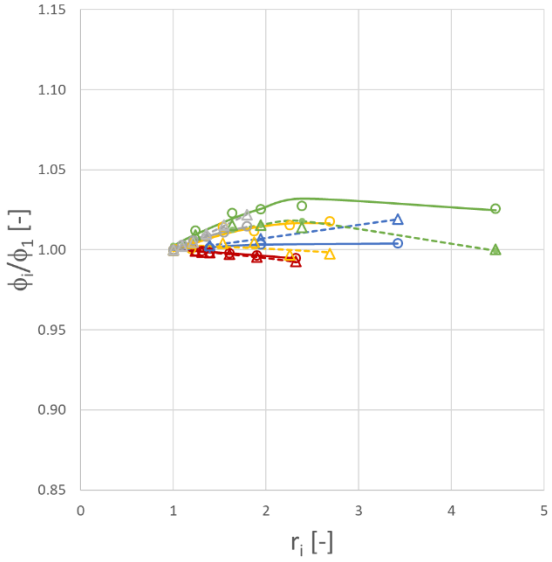

Figure A2. Relative solution convergence with the grid refinement ratio for $\boldsymbol{\phi} = \boldsymbol{C_{Fm}}$(circle) and $\boldsymbol{C_{Fs}}$ (triangle), and $\boldsymbol{\phi_{fit}} = \boldsymbol{C_{Fm}}$ (solid line) and $\boldsymbol{C_{Fs}}$ (dashed line) of VVUA Case No. 1 (red) , 2 (yellow), 3 (blue), 4 (green), and 5 (gray).